Tissue Classification and Segmentation of Pressure Injuries Using Convolutional Neural Networks

Sofia Zahia, Daniel Sierra-Sosa, Begonya Garcia-Zapirain, Adel Elmaghraby

PII: S0169-2607(17)31486-4
DOI: 10.1016/j.cmpb.2018.02.018
Reference: COMM 4635

To appear in: *Computer Methods and Programs in Biomedicine*

Received date: 5 December 2017
Revised date: 30 January 2018
Accepted date: 22 February 2018

Please cite this article as: Sofia Zahia, Daniel Sierra-Sosa, Begonya Garcia-Zapirain, Adel Elmaghraby, Tissue Classification and Segmentation of Pressure Injuries Using Convolutional Neural Networks, *Computer Methods and Programs in Biomedicine* (2018), doi: 10.1016/j.cmpb.2018.02.018

HIGHLIGHTS

- In this paper we presented an approach for automatic tissue segmentation using a Convolutional Neural Network. The methodology is based on the classification of different tissue types: Necrotic, granulation and slough.
- We present different metrics to evaluate our approach, obtaining an overall average classification accuracy of 92.01%, an average total weighted Dice Similarity Coefficient of 91.38%, and an average precision per class of 97.31% for granulation tissue, 96.59% for necrotic tissue, and 77.90% for slough tissue.
- By using this methodology, we were able segment complicated structures within the image to be recognized, providing a robust method for Pressure Injuries assess.

Tissue Classification and Segmentation of Pressure Injuries Using Convolutional Neural Networks

Sofia Zahia[1,2], Daniel Sierra-Sosa[1]*, Begonya Garcia-Zapirain[2] and Adel Elmaghraby[1]

1 Department of Computer Engineering and Computer Science, Duthie Center for Engineering, University of Louisville, Louisville, KY 40292
2 eVida research laboratory, University of Deusto, Bilbao, 48007, SPAIN
* Corresponding author, E-mail: d.sierrasosa@louisville.edu, Tel.:+15028520477

Abstract

Background and Objectives: This paper presents a new approach for automatic tissue classification in pressure injuries. These wounds are localized skin damages which need frequent diagnosis and treatment. Therefore, a reliable and accurate systems for segmentation and tissue type identification are needed in order to achieve better treatment results.
Methods: Our proposed system is based on a Convolutional Neural Network (CNN) devoted to performing optimized segmentation of the different tissue types present in pressure injuries (granulation, slough, and necrotic tissues). A preprocessing step removes the flash light and creates a set of 5x5 sub-images which are used as input for the CNN network. The network output will classify every sub-image of the validation set into one of the three classes studied.
Results: The metrics used to evaluate our approach show an overall average classification accuracy of 92.01%, an average total weighted Dice Similarity Coefficient of 91.38%, and an average precision per class of 97.31% for granulation tissue, 96.59% for necrotic tissue, and 77.90% for slough tissue.
Conclusions: Our system has been proven to make recognition of complicated structures in biomedical images feasible.

Keywords— Deep learning, Pressure injuries, Tissue type classification, Image Segmentation, Convolutional Neural Networks.

I. INTRODUCTION

Pressure injuries are a major concern in a number of countries, the main reasons being the high incidence among elderly and disable patients and the significant expenses for the health care systems. They take the form of localized skin damage which needs frequent diagnosis and treatment (Fig.1). Some researchers attribute these injuries to the quality of acute nursing care resulting in impairment in the patient's quality of life [1]. Pressure injury is assessed and evaluated using manual methods, while parameters such as the area, major and minor diagonal and volume are estimated directly over the wounds [2]. To overcome this difficulty several authors have employed different image processing techniques [3], [4], [5], [6]. These techniques are devoted to evaluating the stage and evolution of the pressure injuries, given morphological features and tissue classification.

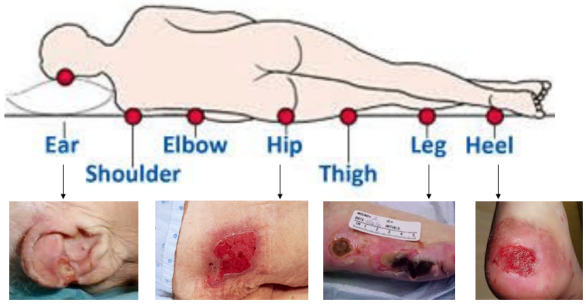

Fig. 1: Different body parts affected by pressure injuries

Image analysis, segmentation and classification problems can be solved using features based on expert knowledge such as Scale-Invariant Feature Transform (SIFT), Speeded Up Robust Features (SURF) and Histogram of Oriented Gradients (HOG) based on a bag of features representation and followed by learning methods such as support Vector machines and Nearest Neighbors, among others [7], [8], [9], [10]. Nonetheless, these techniques are prone to failure when processing complicated structures such as those present in pressure injuries with different tissue types. Therefore, the need for more accurate techniques leads to a new set of learning models based on multiple layers of nonlinear processor units, known as deep learning. In the last few years, deep learning has caught the attention of many researchers when simple methods became insufficient. It has become a fast-growing technique especially in medical image analysis[11].

Deep learning models are widely used for medical image processing. Among these techniques, Convolutional Neural Networks (CNN) and Recurrent Neural Networks (RNN) are the most common, and several types of architecture have been proposed [13], [14], [15], with AlexNet being the most well-known architecture for classification purposes[12].

Several research works have used deep learning for image classification, object detection, segmentation and classification on different types of images [11] such as: brain, retinal, chest x-ray, chest CT, breast, cardiac, abdominal and musculoskeletal images. Conversely, little research has tended to deal with skin lesion images. In [16] authors propose a wound segmentation technique based on a CNN model whose features are then used in infection detection via SVM classifiers and in the healing prediction process via Gaussian Process (GP) Regression. The results show that for wound segmentation, CNN achieved better accuracy compared to the SVM classifier (95% as opposed to 77.6%), whereas for wound infection detection, the SVM classifier trained with CNN features achieved a total accuracy of 84.7%. As for healing prediction, the GP regression model can make long-term future predictions, while [17] also presents a skin lesion segmentation using multi-tract CNN which extends pertained CNNs for multi-resolution skin lesion classification. The results show greater classification accuracy compared to multi-scale approaches. As for [18], the algorithm for skin cancer classification is based on Google′s Inception v3 CNN architecture pre-trained on the 1000 object classes (1.28 million images) of 2014 ImageNet Challenge, in which the final classification layer is retrained with their dataset. The results were also accurate for classification purposes with a level of competence comparable to dermatologists.

Moreover, deep learning models when applied on the other body part images (brain, chest, etc ...) reveal high performance for segmentation and classification. In brain image analysis, the CNN model was used for lesion segmentation [25], [26], [27], [28], tumor segmentation [29], [30], [31] and tissue segmentation [32], [33], [34]. As for RNN, it was used mainly for tissue segmentation [35], [36], while in the case of retinal image analysis, all the results were obtained using CNN and evidenced a high degree of accuracy [19], [20], [21], [22], [23], [24].

In order to achieve accurate tissue segmentation in pressure injuries (stage III and IV), our approach involves using CNN as a deep learning classification technique on a large number of small dataset images. This process is relevant because knowing the tissue type enables the healing process to be assessed and provides medical personnel with a tool for monitoring wound evolution. In section II we describe the Dataset and the proposed architecture, while section III contains results and their discussion which allows us to validate the proposed approach. Lastly section IV summarizes the main works and future perspectives.

II. Methods

A. Dataset

The dataset is made up of 22 images of stage III and IV pressure injuries for training and testing, acquired from the Igurko Hospital, Bilbao-Spain, with 4 being purchased from The National Pressure Ulcer Advisory Panel (NPUAP) online store for validation purposes [38]. The training and test images have a resolution of 1,020x1,020 and were taken using flash due to poor illumination in the nursing facility. The wounds in this dataset are infected, contain necrotic tissue, or are in a healing state evidencing granulation tissue, and all the combinations from tissue types are present in the dataset. These images were automatically cropped in 270,762 RGB matrixes of 5x5x3 in size for granulation tissue, 37,146 for necrotic tissue, and 80,636 for slough. Further details of this process will follow in section II-B.1.

The images were manually segmented using expert knowledge from medical personnel in order to obtain the ground-truth labeling for tissue classification. A control group comprising two physicians was told to independently examine the ground-truth images and document their professional criteria regarding our manual segmentation. The final segmentation was then obtained by merging both the concept from the control group and the originally proposed marked segments.

The four segments selected were labeled as follows: The external skin is represented by a black background (graylevel 0), necrosis by dark gray (graylevel 89), the granulation by light gray (graylevel 170) and slough by white (graylevel 255). The Fig. 2 shows a set of eight original images (1st and 3rd row) and their corresponding ground-truth (2nd and 4th row).

Once the dataset was created, it was divided into 2 parts: training set and testing set. The partition percentage would be around 75% for the training set, and 25% for the testing set as shown in the following table:

	Training	Testing
Granulation	203,072	67,690
Necrosis	27,860	9,286
Slough	60,477	20,159

TABLE I: Number of images for training and testing of CNN architecture

B. Proposed Framework

Unlike the state of the art methods that tend to use a large number of images to train the network to obtain a good segmentation results, our approach involves using a limited number of high resolution images and extracting a larger dataset of small images in order to achieve comparable segmentation of the pressure injury.
Our architecture for image segmentation is comprises a pre-processing step which from a 1,020x1,020 original pressure injury image crops 5x5 images of the different tissue types as output images with their corresponding labels. The choice of small patch size was based on the size limit in which we do not lose the textures belonging to each class, and the average

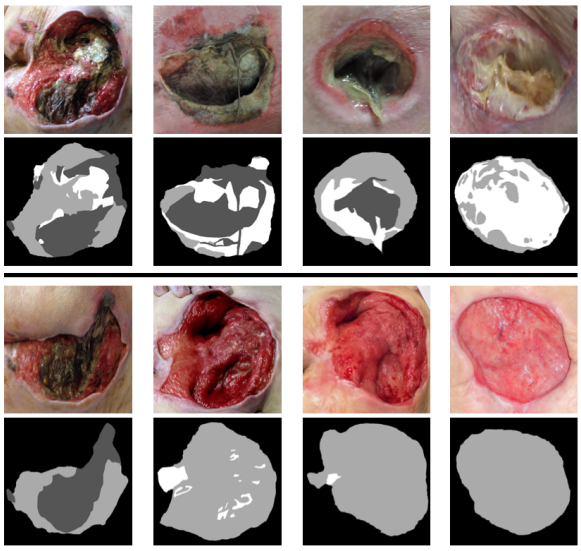

Fig. 2: A set of pressure injury images and their corresponding ground-truth segmentation used to create the dataset and labels

number of pixels defining the boundary between two classes in the images studied.

Once the Convolutional Neural Network is trained, the segmentation of the validation image is then carried out by partitioning the image into 5x5 blocks and classifying each one of them according to the class predicted, from which we construct the segmented image. Fig. 3 sketches our processing workflow for image segmentation.

1) ***Preprocessing****:* The first block in the training step for our system aims at creating the dataset which will be given as input images and their labels to the CNN architecture.

Since our focus is on tissue classification within the wound area we do not address automatic image masking as presented in [2], [43], and a black mask was applied on original pressure injury images in order to retain only the wound area. From the extracted region of interest we then need to remove flash light reflection. To achieve this, we convert the images into grayscale in accordance with the radiometric equation [40]:

$$Y = 0.2126.R + 0.7152.G + 0.0722.B \tag{1}$$

These images are then turned into binary images using Otsu's Method described in [41] where in order to define the white areas.

$$\mu_0 = \sum_{i=0}^{t-1} \frac{ip_i}{\omega_0\,(t)} \tag{2}$$

$$\mu_1 = \sum_{i=t}^{L-1} \frac{ip_i}{\omega_1\,(t)} \tag{3}$$

where $\mu_0(t) = \sum_{i=0}^{t-1} ip_i$ and pi is the probability for the gray scale level i. The mean intensity μ_T is represented as $\mu_T = \omega_0\mu_0 + \omega_1\mu_1,\ \omega_0 + \mu_1 = 1$. The objective is to find t that maximizes

$$J(t) = \sigma_0 + \sigma_1 \tag{4}$$

where $\sigma_0 = \omega_0\ (\mu_0 - \mu_T)^2$ and $\sigma_1 = \omega_1\ (\mu_1 - \mu_T)^2$. By using the threshold $t = 0.95$, each pixel is separated into two classes depending on the amplitude in gray scale values.

Once the binary image has been obtained and flash light zones detected, we then dilate the binary images in order to enlarge these zones. The corresponding zones in the original images are then filled with the value of their boundary pixels in order to retrieve the color of the tissue hidden under the flash light.

Once the flash light artifacts had been removed, the ground-truth was cut into 5x5 images in order to have a larger amount of sub-images, which each one containing only one class. Our database contains 22 of 1020x1020 images and by applying this technique, we ended up with more than 380,000 small images each one containing a part of one of the studied tissue types. This technique represents the proposed solution to enlarge the database. As mentioned previously, the choice of patch size was made for 2 reasons: a smaller size (1x1 for example) would not preserve the textures and would lead to a confusion between the classes subject to study. In addition, the average number of pixels defining a boundary between two classes in the studied images was measured manually and resulted in 5.48 pixels, hence the size 5x5 chosen.
Once we know the label for each one of the patches extracted, we then select the corresponding sub-images in the original images and save them in separate files for the different classes we have at our disposal. The figure below (Fig.4) represents the preprocessing step in our system.

An example from the 5x5 matrices with tissue information is shown in Fig. 5. Note that the matrices labeled as granulation tissue are similar to each other, although the necrotic and slough tissue sub-sets are different. This is due to the fact that necrotic tissue also includes shadows present in the pressure injuries and the slough tissue images have different colors and features because, depending on the bacteria producing the infection, the suppuration color changes.

2) ***Convolutional Neural Networks****:* Convolutional Neural Networks (ConvNet or CNN) have been confirmed as being an enormously successful predictive learning machines and researchers have become more interested in their productive and promising perspective. They are commonly used for speech recognition, object detection and

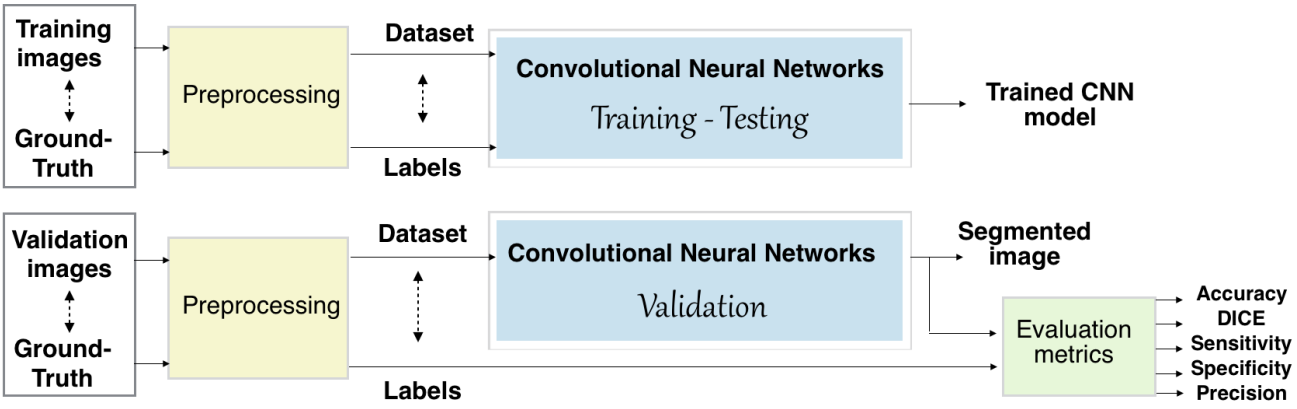

Fig. 3: Proposed architecture for image segmentation using deep learning technique

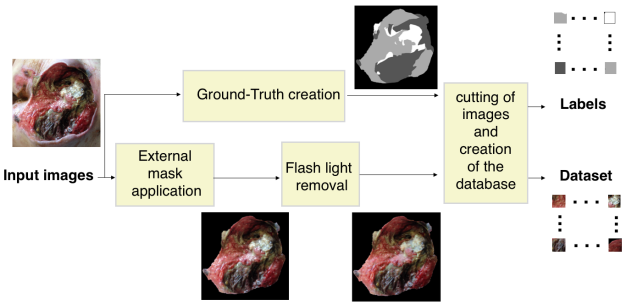

Fig. 4: Preprocessing step for database creation

Fig. 5: Dataset dictionary for the three different tissue types: Granulation, Necrotic and Slough

recognition, among others and can recognize patterns with extreme variability for robustness in terms of distortions and geometric transformations. they generally consist of alternating convolution and non-linear layers, followed by fully connected layers leading into a softmax classifier[42]. These layers are defined as:

- Convolution layer: This is the core building block of a CNN that does most of the computational heavy lifting. It learns the feature localized by the subregions of the input images or the outputs of the previous layer before it. The convolution layer has different features:
  - The filter size indicates the size of the subregions being computed with the filter.
  - The stride is the step size with which the filter moves all over the image. In some types of architecture, when the stride is higher than 1, it replaces the max-pooling layer that reduces the output size.
  - The number of filters determines the number of channels in the convolution layer output.
  - Zero-padding is an action that involves adding borders vertically and horizontally to the input image, and this is generally done to preserve the spatial size of the input so that input and output width and height are the same.

  Usage of all these features is depicted in Fig. 6, where we illustrate the process in order to obtain an output image by using the convolution filter on a zero-padded input image to preserve its dimensions [39].

- Pooling layer: this operates independently on every slice of the input and resizes it spatially, using the MAX operation. Pooling layers aim at decreasing the number of parameters needed to characterize layers deeper in the network and at reducing the number of computations needed for training the network.

- Fully connected layer: this layer gathers all the neurons together. Hence, it combines all the features previously learned to classify the images. The output size of this layer is then equal to the number of classes being studied.

- Softmax layer: known as normalized exponential, this is an activation function which follows the fully connected layer for multi-class classification purposes.

- Classification layer: this assigns the output result of the Softmax layer to one of the studied classes by using the cross entropy function.

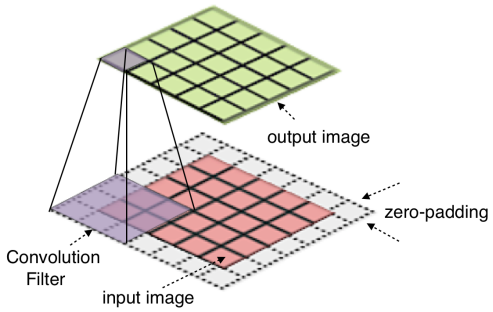

Fig. 6: Illustration of the convolution layer with a filter size 3x3 and a zero-padding 1x1 [39]

Our system is made up of of 9 layers: 3 convolution layers where the first two are with zero-padding (2x2 and 1x1), and each one is followed by a Rectified Lineal Unit (ReLU1, ReLU2 and ReLU3). The number of feature maps and weights in each convolution layer is 10,20,30 and 760,560,840 respectively. Each feature map detects one kind of features across the image. The choice of filter size was made so as to preserve the textures that belong to each different tissue type in the pressure injury. The fully connected layer is then followed by a Softmax Layer, ending with a classification layer which gives rise to the probability of patch belonging to one of the 3 predicted classes, as shown in Fig. 7. The algorithm was coded on Matlab 2017a using Neural Network Toolbox.

III. Results

A. Validation metrics

The segmentation method was evaluated using five performance measures: accuracy, Dice Similarity Coefficient (DSC), sensitivity, specificity and precision [44] . To explain these metrics, the different regions that are generated when comparing the ground truth with the segmented results obtained are shown in Fig.8. The True Positive (TP) region refers to those pixels that were correctly classified in a targeted class, the False Positive (FP) region refers to those pixels mistakenly classified as belonging to the targeted class and the False Negative (FN) region refers to those pixels belonging to the targeted class that were not classified in that class, while the True Negative (TN) region refers to those pixels that do not belong to the target class and are excluded.

- **Accuracy**: the segmentation accuracy is the ratio of the number of pixels accurately clustered by the algorithm out of the total number of pixels segmented.

- **Dice Similarity Coefficient (DSC)**: this is measured for each class segmentation considered apart, and also for the whole segmentation, by calculating the sum of weighted dice similarity coefficients of each class as follows:

$$\mathbf{DSC} = \frac{\mathbf{2|Ground\_truth \cap Detection|}}{\mathbf{|Ground\_truth| + |Detection|}} \quad (5)$$

The weighted DSC for the whole segmentation is as follows:

$$\mathbf{DSC_w} = \sum_{\mathbf{i=1}}^{\mathbf{n}} \mathbf{DSC_i} \times \mathbf{w_i} \quad (6)$$

where DSC_i is the DSC corresponding to each class when measured alone, and w_i is a ratio of the number of pixels in the class i out of the sum of pixels of all the classes.

- **Sensitivity**: also named "recall", this represents the ratio of class pixels accurately segmented out of the union of ground-truth same class pixels.

$$\textbf{Sensitivity} = \frac{\mathbf{TP}}{\mathbf{TP + FN}} \quad (7)$$

- **Specificity**: this represents the ratio of negatives that are correctly identified.

$$\textbf{Specificity} = \frac{\mathbf{TN}}{\mathbf{TN + FP}} \quad (8)$$

For exact segmentation sensitivity, specificity and total DSC should be equal to one.

- **Precision**: this represents the ratio of a class pixels accurately clustered out of the union of segmented same-class pixels.

$$\textbf{Precision} = \frac{\mathbf{TP}}{\mathbf{TP + FP}} \quad (9)$$

B. Results

The significant advantage of our proposed approach lies in its capability to accurately segment the wound's different tissue types. We measure the performance of our proposal for both the classification and the segmentation tasks, and the accuracy of the classification of the different 3 types of tissue was 92.01% . Classification from these masks allows us to perform image segmentation in spite of the adverse registry conditions such as diverse illumination conditions and image distortion, among others.

The results for the segmentation task are presented for the pressure injuries depicted in Fig. 9 are shown in Tables I through V. Each of these tables corresponds to columns (a) to (d) of Fig.9 respectively.
We obtained the validation metrics shown in section III for the tissue classes. Note that in Fig. 9 (a) and (c) the pressure injuries contain the three tissue classes, whereas Fig. 9 (b) only contain granulation tissue and in Fig. 9 (d) the wound contain granulation and slough tissue classes.

In particular, in the TABLE II and TABLE IV corresponding to Fig. 9 (a) and Fig. 9 (c) we provide

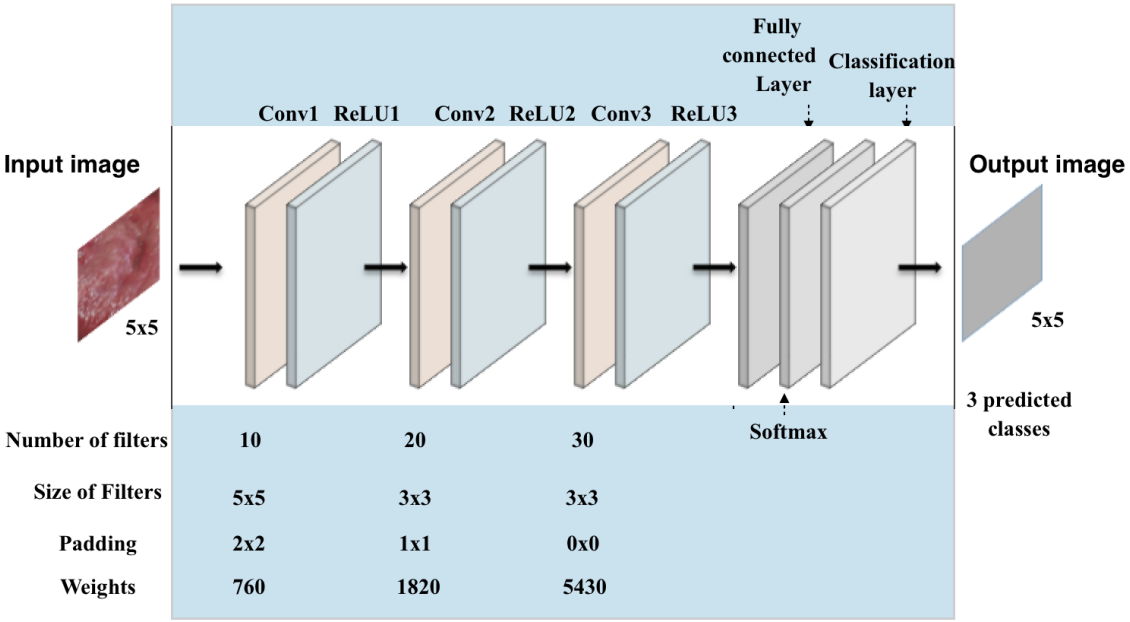

Fig. 7: Proposed Convolutional Neural Network architecture for image segmentation

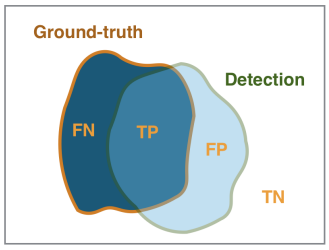

Fig. 8: Illustration of different segmentation areas for performance metrics measurement

the results for the segmentation of the three different tissue classes. In Fig 9 (a) we achieved a DSC of 96.34% for granulation via the proposed system, 97.49% for necrosis and 65.03 for slough classes; in Fig 9 (c) we achieved a DSC of 96.91% for granulation, 86.15% for necrosis and 61.67 for slough classes.

Note that, slough tissue was partly misclassified because there are different textures related to it. Depending on the different types of bacteria, the infection generated by slough tissue has different colors such as off-white, green, light yellow and dark yellow, which can confuse the system. In the TABLE III we show the results when only granulation tissue is contained in the wound, and in this case we achieve a DSC of 98.35% for this kind of tissue. The results obtained when two classes of tissue are contained in the wound are shown in TABLE V, and in this case the injury contains granulation and slough, each of them classified by the system with DSCs of 96.73% and 81.19% respectively.

With this system we obtained an average DSC_w of 91.38%, and an average precision per class of 97.31% for granulation tissue, 96.59% for necrotic tissue, and 77.90% for slough tissue. The sensitivity and specificity for all examples were also computed for each tissue type in each case, and the tissue segmentation processing times were also evaluated, with these times ranging from 46 to 83 seconds on an Intel® Core™ i7-5500 CPU at 2.40 GHz an NVIDIA® GeForce® GTX 780 graphics card.

	Predicted tissue types		
Evaluation metrics	Granulation	Necrosis	Slough
DSC	96.34	97.49	65.03
Sensitivity	94.83	96.79	60.33
Specificity	97.52	95.48	98.92
Precision	97.72	94.08	72.62
DSC_w	95.49		
Processing time	61s		

TABLE II: Results of the segmentation of image Fig 9 (a) containing granulation, slough and necrosis

	Predicted tissue types		
Evaluation metrics	Granulation	Necrosis	Slough
DSC	98.35	N/A	N/A
Sensitivity	98.29	N/A	N/A
Specificity	N/A	99.99	99.74
Precision	100	N/A	N/A
DSC_w	98.35		
Processing time	56s		

TABLE III: Results of the segmentation of image Fig 9 (b) containing only granulation

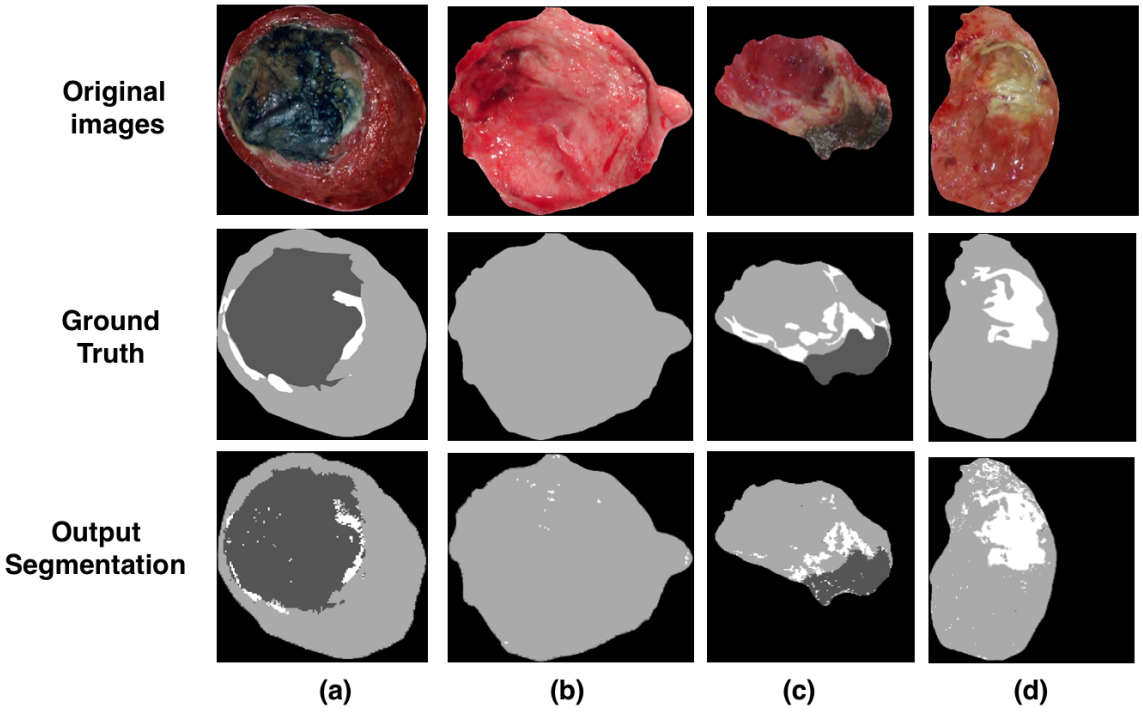

Fig. 9: Examples of original images and their corresponding ground-truth and output segmentation using deep learning

	Predicted tissue types		
Evaluation metrics	Granulation	Necrosis	Slough
DSC	96.91	86.15	61.67
Sensitivity	98.11	94.57	58.12
Specificity	70.99	99.48	98.05
Precision	92.65	99.11	80.01
DSC_w	87.74		
Processing time	46s		

TABLE IV: Results of the segmentation of image Fig 9 (c) containing granulation, slough and necrosis

	Predicted tissue types		
Evaluation metrics	Granulation	Necrosis	Slough
DSC	96.73	N/A	81.19
Sensitivity	81.66	N/A	95.49
Specificity	95.53	99.93	82.87
Precision	98.87	N/A	81.09
DSC_w	83.94		
Processing time	83s		

TABLE V: Results of the segmentation of image Fig 9 (d) containing only granulation and slough

IV. Discussion

Despite the fact that our method for pressure injury tissue classification was used on a different database from the ones used in the state of the art techniques, our results provided compelling evidence that the strategy proposed is more reliable when compared to other research reported, with regard to their image segmentation approaches. Skin wound segmentation research was previously carried out using machine learning and other methods and revealed good results.

R. Mukherjee et al. proposes segmentation performed by converting the RGB images to HSI, then using Fuzzy Divergence Based Thresholding and mathematical morphology operations combined [7]. As for classification, they use color and textural features exacted from fifteen color spaces, and the color-based features were namely: mean, standard deviation, skewness, kurtosis and variance. Conversely, ten textural features were extracted: Shannons entropy, three local contrast features and six local binary pattern features. Regarding the classification algorithms, they used Bayesian and Support Vector Machine algorithms to classify the three major part of the wound: granulation, slough and necrosis. The results showed an overall accuracy of 87.61%.

F. J. Veredas et al. chose to combine the mean-shift smoothing procedure and the region-growing algorithm for the segmentation and carried out tissue-type classification using three different machine learning methods namely: Neural Networks, Support Vector Machine and Random-Forest decision trees[9]. The evaluation metrics showed an overall accuracy of 88.08% using SVM classification method with their database,as compared to 92.01% using our approach and database.
Thus, Our proposed system will enable physicians and medical staff to assess pressure injuries efficiently by providing them with accurate measurements of

the different tissue types present in the wounds, and consequently predicting their healing progress and examine the effectiveness of the applied treatment.

However, the model has some limitations. Due to depth in some pressure injuries, there are some parts that appear dark in the images. Our system then confuses them with necrotic tissue, which is generally very dark in color. Several classes of infections also exist that are produced by different bacteria, and the slough tissue color changes depending on the kind of the bacteria. These changes affect the classification and should be split depending on the bacteria producing the infection in question.

V. Conclusion

We have presented an approach for automatic tissue segmentation using a Convolutional Neural Network. As the proposed methodology is based on the classification of different tissue types (necrotic, granulation and slough), it enables complicated structures within the image to be recognized. By using this methodology we were able to obtain very good results and demonstrate that the proposed method is robust in terms of the various aspects that the same tissue type may have, with minimum preprocessing and no post-processing. Thanks to the promising results obtained, we are sure that our system will enable clinicians to assess a wound's healing using the accurate tissue measurements provided, and to differentiate from among the wound's composition, which is an essential step in pressure injury diagnosis. We are currently working on expanding our dataset in order to be able to include new different classes for classification purposes, such as depths and shadows in the wound, healing skin on the injury boundary and color addressing of infection, among others. Adding more pressure injury images from all body parts (sacral, ischium, gluteus, hips, and heels of all bed-bound patients and also diabetic foot) and with different tissue types will increase the efficiency of the classification. By having more images of the studied classes, the system will be able to better recognize the textures of the tissue types, especially slough which has many textures depending on the bacteria causing the infection. We are currently working on increasing our database by capturing new high quality images of pressure injuries from cooperative hospitals. The proposed methodology is useful not only for the assessment of pressure injuries but also other skin conditions and for the segmentation and classification of images based on class texture.

VI. Acknowledgment

This project has been funded by the University of Louisville Computer Engineering and Computer Science Department. The authors would like to thank the Igurko Hospital in Bilbao, Spain, for the images provided in order to carry out this work. Acknowledgment to Basque country government that partially funded this project with IT905-16 grant.

References

[1] Tubaishat, A., Papanikolaou, P., Anthony, D., and Habiballah, L. (2017). Pressure Ulcers Prevalence in the Acute Care Setting: A Systematic Review, 2000-2015. Clinical Nursing Research, 1054773817705541.

[2] Ortiz, D. P., Sierra-Sosa, D., and Zapirain, B. G. (2017). Pressure ulcer image segmentation technique through synthetic frequencies generation and contrast variation using toroidal geometry. Biomedical engineering online, 16(1), 4.

[3] Leachtenauer, J., Kell, S., Turner, B., Newcomer, C., Lyder, C., Alwan, M. (2006, August). A non-contact imaging-based approach to detecting stage I pressure ulcers. In Engineering in Medicine and Biology Society, 2006. EMBS'06. 28th Annual International Conference of the IEEE (pp. 6380-6383). IEEE.

[4] Guadagnin, R., Neves, R. D. S., Santana, L. A., Guilhem, D. B. (2014). An image mining based approach to detect pressure ulcer stage. Pattern recognition and image analysis, 24(2), 292-296.

[5] Hansen, G. L., Sparrow, E. M., Kokate, J. Y., Leland, K. J., Iaizzo, P. A. (1997). Wound status evaluation using color image processing. IEEE Transactions on Medical Imaging, 16(1), 78-86.

[6] Mankar, N. B., Nagdeve, U. (2013). Comparison of different imaging techniques used for chronic wounds. IJRET, 2(7), 68-70.

[7] Mukherjee, R., Manohar, D. D., Das, D. K., Achar, A., Mitra, A., and Chakraborty, C. (2014). Automated tissue classification framework for reproducible chronic wound assessment. BioMed research international, 2014.

[8] Bedo, M. V. N., Santos, L. F. D., Oliveira, W. D., Blanco, G., Traina, A. J. M., Frade, M. A., ... and Junior, C. T. (2015, June). Color and texture influence on computer-aided diagnosis of dermatological ulcers. In Computer-Based Medical Systems (CBMS), 2015 IEEE 28th International Symposium on (pp. 109-114). IEEE.

[9] Veredas, F. J., Luque-Baena, R. M., Martín-Santos, F. J., Morilla-Herrera, J. C., and Morente, L. (2015). Wound image evaluation with machine learning. Neurocomputing, 164, 112-122.

[10] Arroyo, J. L. G., Zapirain, B. G., and Zorrilla, A. M. (2011, December). Blue-white veil and dark-red patch of pigment pattern recognition in dermoscopic images using machine-learning techniques. In Signal Processing and Information Technology (ISSPIT), 2011 IEEE International Symposium on (pp. 196–201). IEEE.

[11] Litjens, G., Kooi, T., Bejnordi, B. E., Setio, A. A. A., Ciompi, F., Ghafoorian, M., ... and Sánchez, C. I. (2017). A survey on deep learning in medical image analysis. arXiv preprint arXiv:1702.05747.

[12] Krizhevsky, A., Sutskever, I., Hinton, G., 2012. Imagenet classification with deep convolutional neural networks. In: Advances in Neural Information Processing Systems. pp. 1097–1105.

[13] Simonyan, K., Zisserman, A., 2014. Very deep convolutional networks for large-scale image recognition. arXiv:1409.1556.

[14] Szegedy, C., Liu, W., Jia, Y., Sermanet, P., Reed, S., Anguelov, D., Erhan, D., Vanhoucke, V., Rabinovich, A., 2014. Going deeper with convolutions. arXiv:1409.4842.

[15] He, K., Zhang, X., Ren, S., Sun, J., 2015. Deep residual learning for image recognition. arXiv:1512.03385.

[16] Wang, C., Yan, X., Smith, M., Kochhar, K., Rubin, M., Warren, S. M., ... and Lee, H. (2015, August). A unified framework for automatic wound segmentation and analysis with deep convolutional neural networks. In Engineering in Medicine and Biology Society (EMBC), 2015 37th Annual International Conference of the IEEE (pp. 2415-2418). IEEE.

[17] Kawahara, J., and Hamarneh, G. (2016, October). Multi-resolution-Tract CNN with Hybrid Pretrained and Skin-Lesion Trained Layers. In International Workshop on Machine Learning in Medical Imaging (pp. 164-171). Springer International Publishing.

[18] Esteva, A., Kuprel, B., Novoa, R. A., Ko, J., Swetter, S. M., Blau, H. M., and Thrun, S. (2017). Dermatologist-level classification of skin cancer with deep neural networks. Nature, 542(7639), (115–118).

[19] Fu, H., Xu, Y., Lin, S., Wong, D. W. K., and Liu, J. (2016, October). Deepvessel: Retinal vessel segmentation via deep learning and conditional random field. In International Conference on Medical Image Computing and Computer-Assisted Intervention (pp. 132–139). Springer International Publishing.

[20] Fu, H., Xu, Y., Wong, D. W. K., and Liu, J. (2016, April). Retinal vessel segmentation via deep learning network and fully-connected conditional random fields. In Biomedical Imaging (ISBI), 2016 IEEE 13th International Symposium on (pp. 698–701). IEEE.

[21] Maninis, K. K., Pont-Tuset, J., Arbeláez, P., and Van Gool, L. (2016, October). Deep retinal image understanding. In International Conference on Medical Image Computing and Computer-Assisted Intervention (pp. 140–148). Springer International Publishing.

[22] Wu, A., Xu, Z., Gao, M., Buty, M., and Mollura, D. J. (2016, April). Deep vessel tracking: A generalized probabilistic approach via deep learning. In Biomedical Imaging (ISBI), 2016 IEEE 13th International Symposium on (pp. 1363–1367). IEEE.

[23] Zilly, J., Buhmann, J. M., and Mahapatra, D. (2017). Glaucoma detection using entropy sampling and ensemble learning for automatic optic cup and disc segmentation. Computerized Medical Imaging and Graphics, 55, 28–41.

[24] Gao, X., Lin, S., and Wong, T. Y. (2015). Automatic feature learning to grade nuclear cataracts based on deep learning. IEEE Transactions on Biomedical Engineering, 62(11), 2693–2701.

[25] Birenbaum, A., and Greenspan, H. (2016, October). Longitudinal multiple sclerosis lesion segmentation using multi-view convolutional neural networks. In International Workshop on Large-Scale Annotation of Biomedical Data and Expert Label Synthesis (pp. 58–67). Springer International Publishing.

[26] Brosch, T., Tang, L. Y., Yoo, Y., Li, D. K., Traboulsee, A., and Tam, R. (2016). Deep 3D convolutional encoder networks with shortcuts for multiscale feature integration applied to multiple sclerosis lesion segmentation. IEEE transactions on medical imaging, 35(5), 1229–1239.

[27] Ghafoorian, M., Karssemeijer, N., Heskes, T., van Uden, I., Sanchez, C., Litjens, G., de Leeuw, F.-E., van Ginneken, B., Marchiori, E., Platel, B., 2016a. Location sensitive deep convolutional neural networks for segmentation of white matter hyperintensities. arXiv:1610.04834.

[28] Ghafoorian, M., Karssemeijer, N., Heskes, T., van Uder, I. W. M., de Leeuw, F. E., Marchiori, E., ... and Platel, B. (2016, April). Non-uniform patch sampling with deep convolutional neural networks for white matter hyperintensity segmentation. In Biomedical Imaging (ISBI), 2016 IEEE 13th International Symposium on (pp. 1414–1417). IEEE.

[29] Havaei, M., Davy, A., Warde-Farley, D., Biard, A., Courville, A., Bengio, Y., ... and Larochelle, H. (2017). Brain tumor segmentation with deep neural networks. Medical image analysis, 35, 18–31.

[30] Havaei, M., Guizard, N., Chapados, N., and Bengio, Y. (2016, October). HeMIS: Hetero-modal image segmentation. In International Conference on Medical Image Computing and Computer-Assisted Intervention (pp. 469–477). Springer International Publishing.

[31] Kamnitsas, K., Ledig, C., Newcombe, V. F., Simpson, J. P., Kane, A. D., Menon, D. K., ... and Glocker, B. (2017). Efficient multi-scale 3D CNN with fully connected CRF for accurate brain lesion segmentation. Medical image analysis, 36, 61–78.

[32] Zhang, W., Li, R., Deng, H., Wang, L., Lin, W., Ji, S., and Shen, D. (2015). Deep convolutional neural networks for multi-modality isointense infant brain image segmentation. NeuroImage, 108, 214–224.

[33] Chen, H., Dou, Q., Yu, L., Heng, P.-A., 2016a. VoxResNet: Deep voxelwise residual networks for volumetric brain segmentation. arXiv:1608.05895.

[34] Moeskops, P., Viergever, M. A., Mendrik, A. M., de Vries, L. S., Benders, M. J., and Išgum, I. (2016). Automatic segmentation of MR brain images with a convolutional neural network. IEEE transactions on medical imaging, 35(5), 1252–1261.

[35] Stollenga, M. F., Byeon, W., Liwicki, M., and Schmidhuber, J. (2015). Parallel multi-dimensional lstm, with application to fast biomedical volumetric image segmentation. In Advances in Neural Information Processing Systems (pp. 2998–3006).

[36] Andermatt, S., Pezold, S., and Cattin, P. (2016, October). Multi-dimensional gated recurrent units for the segmentation of biomedical 3D-data. In International Workshop on Large-Scale Annotation of Biomedical Data and Expert Label Synthesis (pp. 142–151). Springer International Publishing.

[37] Guadagnin, R., Neves, R. D. S., Santana, L. A., and Guilhem, D. B. (2014). An image mining based approach to detect pressure ulcer stage. Pattern recognition and image analysis, 24(2), 292–296.

[38] http://www.npuap.org/online-store/

[39] https://leonardoaraujosantos.gitbooks.io/artificial-inteligence/content/convolutional_neural_networks.html

[40] Bovik, A. C. (2010). Handbook of image and video processing. Academic press.

[41] Raja, N., Rajinikanth, V., Latha, K. (2014). Otsu based optimal multilevel image thresholding using firefly algorithm. Modelling and Simulation in Engineering, 2014, 37.

[42] Murphy, J. (2016). An Overview of Convolutional Neural Network Architectures for Deep Learning.

[43] Rickard, H. E., Tourassi, G. D., and Elmaghraby, A. S. (2003, April). Self-organizing maps for masking mammography images. In Information Technology Applications in Biomedicine, 2003. 4th International IEEE EMBS Special Topic Conference on (pp. 302–305). IEEE.

[44] Litjens, G., Kooi, T., Bejnordi, B. E., Setio, A. A. A., Ciompi, F., Ghafoorian, M., ... and Sánchez, C. I. (2017). A survey on deep learning in medical image analysis. arXiv preprint arXiv:1702.05747.